Journal of Pure and Applied Mathematics: Advances and Applications
Volume 10, Number 2, 2013, Pages 191-226

NEW RESULTS ON MATHEMATICAL MODELLING AND SIMULATION OF SEMI ACTIVE SUSPENSION SYSTEMS WITH MAGNETO-RHEOLOGICAL DAMPER

DIMUTHU DHARSHANA ARACHCHIGE, SUBODHA THARANGI IRESHIKA, ORESTE NYNIYONSABA and HAMID REZA KARIMI

Department of Engineering
Faculty of Engineering and Science
University of Agder
4879, Grimstad
Norway
e-mail: hamid.r.karimi@uia.no

Abstract

Magneto-rheological (MR) dampers are being developed for a wide variety of applications where controllable damping is desired. These applications include dampers for construction industry, automobiles, heavy trucks, bicycles, prosthetic limbs, gun recoil systems, and possibly others. Semi active suspension (SAS) with MR dampers are used to isolate the system from the undesirable vibration sources. The MR dampers provide a controlled torque through control of an applied magnetic field. The magnetic field is controlled by an input current and it has been found that the torque current behaviour of the MR damper is highly nonlinear.

The research aims to analyze the nonlinear behaviour of an MR damper occupied in the SAS laboratory platform. Firstly, the SAS system is mathematically modelled to obtain governing equations of the damping torque and subsequently, stability of the system is investigated. One of the premier model proposed to analyze the MR damper; Bouc-Wen model, is discussed by analyzing the effect of parameters on the hysteresis behaviour. Thereafter,

2010 Mathematics Subject Classification: 00A72, 74H45, 34C55.

Keywords and phrases: vibration, magneto-rheological (MR), Bouc-Wen, hysteresis.

Received August 9, 2013

Bouc-Wen model is integrated to the SAS platform and the effect of the parameters to the vibration response is analyzed. Subsequently, experimental results are compared with the results of the proposed theoretical model. Consequently, it is concluded that MR rotary damper effectively enables to eliminate or reduce the undesirable vibrations by controlling the SAS damping torque in a continuous way.

1. Introduction

In any mechanism, there is a potential for extraneous energy to be created beyond what it is needed. In most systems, that excess energy becomes a problem. Typically, the energy that is created becomes vibration. The presence of vibration leads to excessive wear of bearings, formation of cracks, loosening of fasteners, structural and mechanical failures, frequent and costly maintenance of machines, electronic malfunctions and exposure of humans leads to pain, discomfort and reduced efficiency. Hence, it is necessary to eliminate or reduce vibration. A vibration isolation system occupied with dampers can be used to reduce vibrations, which convert this excess energy into heat which is then dissipated. Currently available vibration isolation systems can be categorized into three main types as active, passive, and semi-active.

1.1. Passive isolation

The restoring and dissipative forces in a passive vibration control system are generated purely due to the relative deflection and relative velocity across the passive elements, such as springs and dampers of various types. Passive vibration isolation systems thus do not require any external power source and offer simple, inexpensive, and reliable means to achieve vibration control. However, passive vibration isolation systems possess inherent performance limitations due to their fixed parameters, such as damping.

1.2. Active isolation

The control forces in an active vibration control system are generated via active force generators, and change with variations in excitation and response characteristics. Active vibration control systems can supply energy as well as dissipate energy when required, whereas passive

systems can only dissipate or temporarily store energy. The major disadvantages of active vibration control systems include the requirement of an external energy source and a sophisticated control system with number of sensors.

1.3. Semi-active isolation (SAS)

Semi-active vibration isolation systems generate damping forces passively, while the damping parameters are modulated by using an active control system. Semi-active vibration control systems offer an excellent compromise between the performance benefits of active systems and the simplicity of passive vibration systems. These vibration systems require only low electrical power for necessary signal processing and can provide improved vibration isolation performance as compared with that of passive ones.

2. The Magneto-Rheological (MR) Damper

An MR damper is a semi-active control device that uses MR fluid to produce controllable damper. The MR damper looks like a normal damper, but has surrounding coils. These coils make it possible to set up a magnetic field through the fluid. The magnetic field can be controlled by an active/semi-active or passive controlled current. The inherent feature for the MR damper is high non-linear dynamic behaviour including hysteresis. The main benefits of the MR damper are low-voltage and current demands, precise and instantaneous control, continuously variable damping and simple electronics.

2.1. MR fluid

The MR fluid is composed of oil and varying percentages of iron particles that have been coated with an anti-coagulant material [4]. When inactivated, MR fluid behaves as ordinary oil. When exposed to a magnetic field, micron-size iron particles that are dispersed throughout the fluid align themselves along magnetic flux lines [5]. This reordering of iron particles can be visualized as a large number of microscopic spherical beads that are threaded onto a very thin string. Once aligned in

this fashion, the iron particles resist being moved out of their respective flux lines and act as a barrier to fluid flow. This phenomenon is illustrated in the Figures 1 and 2 [11].

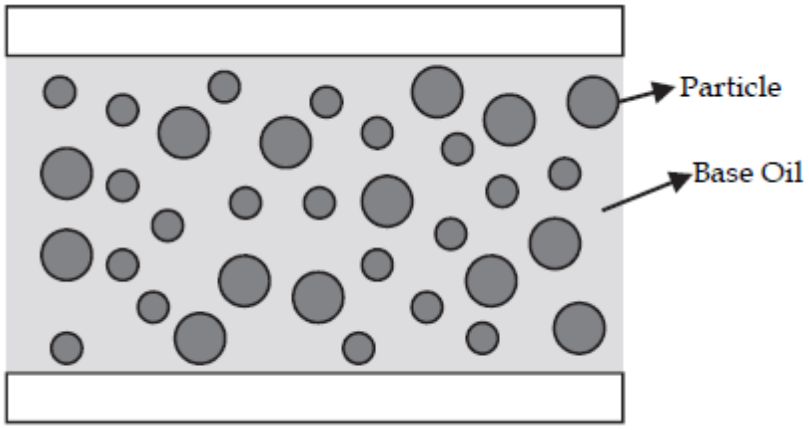

Figure 1. MR fluid when no magnetic field applied [11].

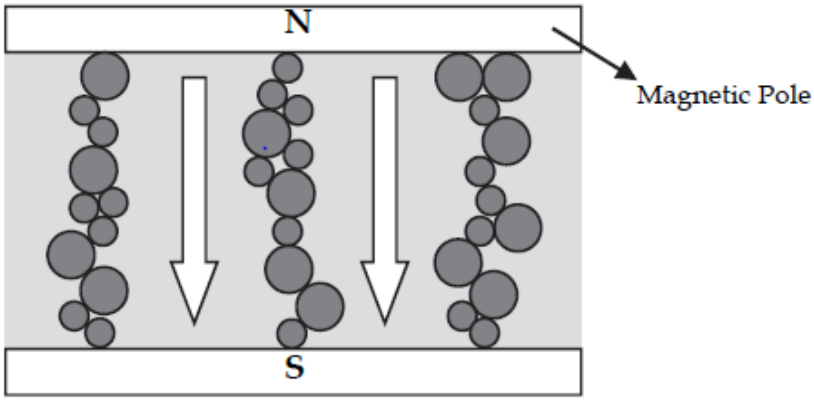

Figure 2. MR fluid when magnetic field applied [11].

By changing the current, the strength of the magnetic field can be controlled, thus change in fluid viscosity. It has been proved that, this change is approximately linear to the control current.

2.2. Modes of operation of MR fluid

MR fluid can be used in three different ways, all of which can be applied to MR damper design depending on the damper's intended use. These modes of operation are referred to as squeeze mode, valve mode, and shear mode [6].

2.2.1. Squeeze mode

Two magnetic pole plates are squeezed together on a thin film of MR fluid as shown in Figure 3(a). The applied force is parallel to the direction of flux lines and it pressurizes the chain-like structures of MR fluid particles [6].

2.2.2. Shear mode

Shear mode has two magnetic pole plates move relative to each other, thus 'shearing' the fluid between them as depicted in Figure 3(b). The applied magnetic field places the MR particles perpendicular to the pole plate, while the shearing attempts to bend the particle chain along the flux lines. When the magnetic field increases, the resistance to shearing also increases. Usually, the shear mode is used in low force dampers and also used as magnetic brakes and clutches [6].

2.2.3. Valve mode

The valve mode is also known as the pressure driven mode. The pressurized MR fluid flows through fixed magnetic poles as per the Figure 3(c). When magnetic field is applied, the MR particles are aligned parallel to the magnetic field lines and it resists flow of the pressurized MR fluid. It is called 'valve mode' because its function is similar to operation of a valve. Pressure driven flow mode is the probably most common mode used in applications [6].

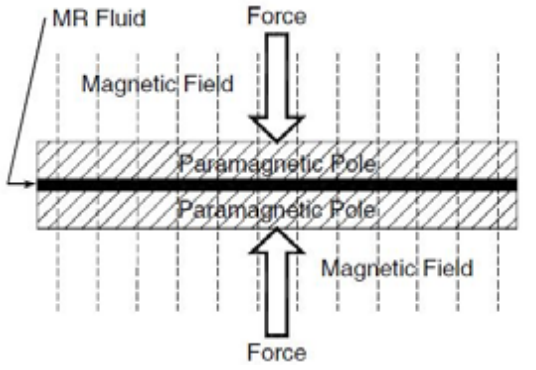

(a)

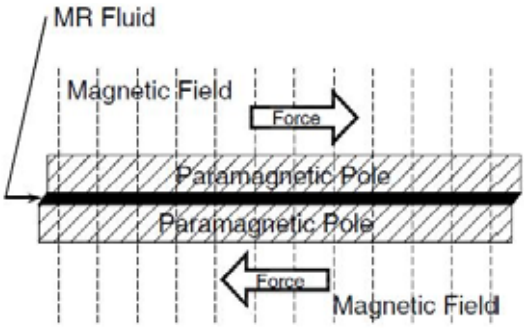

(b)

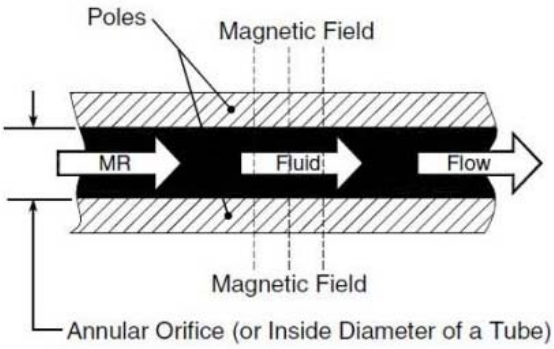

(c)

Figure 3. MR fluid used in (a) squeeze mode; (b) shear mode; and (c) valve mode operation [6].

2.3. Types of MR dampers

2.3.1. Mono tube

A mono tube MR damper has only one reservoir for the MR fluid and the change in volume allows moving the piston rod. In order to accommodate change in reservoir volume, an accumulator piston is usually used [6]. The accumulator piston provides a barrier between the MR fluid and a compressed gas (usually nitrogen) that is used to accommodate the necessary volume changes.

2.3.2. Twin tube

The twin tube MR damper is one that has two fluid reservoirs, one inside of the other. This configuration has an inner and an outer housing. The inner housing filled with MR fluid guides the piston rod assembly just as the housing of a mono tube damper does [6].

2.3.3. Double-ended

The double ended MR damper is one that has piston rods of the same diameter that protrude through both ends of the damper. Since there is no change in volume as the piston rod moves, the double-ended damper does not require an accumulator or other similar device [6].

2.4. MR rotary damper

MR rotary damper, as the name suggests, is used when rotary motion needs damping. There exist several types of rotary dampers, but the one that is used in semi active suspension (SAS) platform is the disk brake [9]. The disk brake is one of the most commonly used rotary dampers. It has a disk shape and contains MR fluid and a coil as shown in Figure 4 [9].

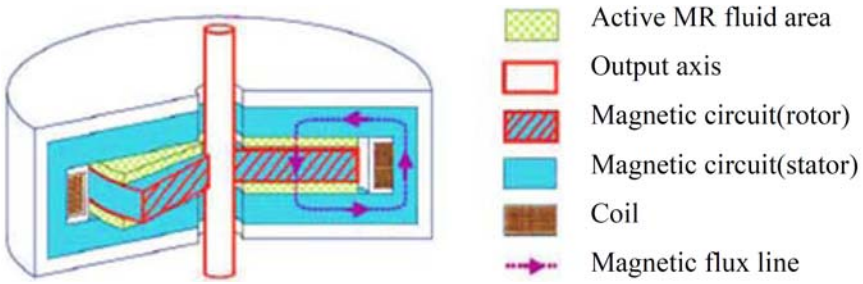

Figure 4. MR rotary damper-disk brake [9].

The chamber (active MR fluid area) where rotor rotates, is filled with MR fluid and the viscosity is changed due to the generated magnetic field of the coil, affecting to control the torque of the output axis [9].

3. Semi Active Suspension (SAS) System with MR Rotary Brake

The laboratory SAS system is mainly operated by a DC motor with gear coupled to a wheel, which is eccentrically fixed with the frame. The suspended car wheel rotates with the contact of the small wheel and oscillates up and down with the effect of wheel eccentricity. The system consists of a rotary MR damper, three encoders, pre-programmed control algorithms, and the mechanical structure [8].

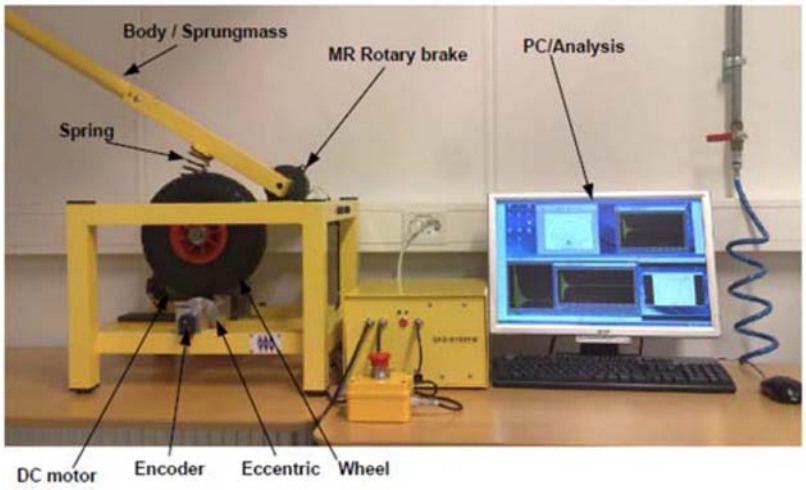

Figure 5. SAS system-laboratory platform [8].

3.1. Mathematical modelling of the SAS system

The behaviour and performance of the system consisting rigid and flexible parts are analyzed by using dynamic mathematical model of displacement motions.

3.1.1. Analysis of the spring

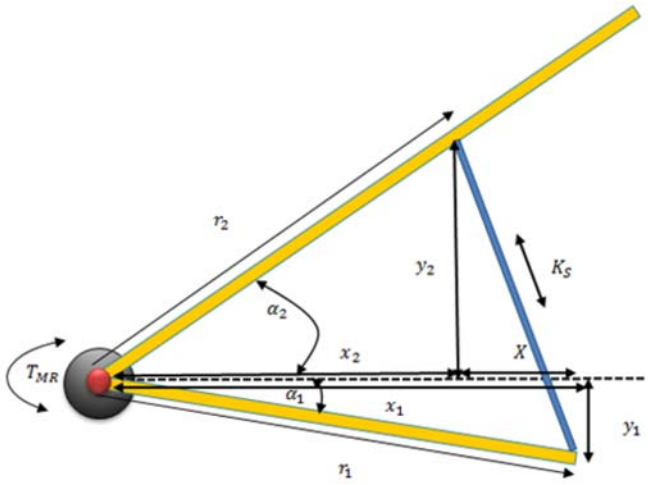

Figure 6. Geometry view of the beams [8].

Momentum on the MR damper due to the stiffness of the spring [8];

$$M_{T_{MR}} = r_2 K_s (l_{os} - \sqrt{X^2 + (y_2 - y_1)^2}), \quad (1)$$

$$M_{T_{MR}} = r_2 K_s (l_{os} - \sqrt{(r_1 \mathrm{Cos}\,\alpha_1 - r_2 \mathrm{Cos}\,\alpha_2)^2 + (r_2 \mathrm{Sin}\,\alpha_2 - r_1 \mathrm{Sin}\,\alpha_1)^2}), \quad (2)$$

where

α_1: The angle between the upper beam and horizontal line (-3.653^{o} [8]).

α_2: The angle between the lower beam and horizontal line (31.814^{o} [8]).

β: The angle to the horizontal between the line drawn through the centers of the tire and MR damper (0.2337 rad [8]).

K_s: The elasticity coefficient of the spring $(3333 \mathrm{Nm}^{-1}$ [8]).

l_{os}: The length of the no load spring $(0.125 \mathrm{m}$ [8]).

l_0: The length of the loaded spring (0.075m [8]).

r_1: The distances between the spring mount and the lower beam (0.2712m [8]).

r_2: The distances between the spring mount and the upper beam (0.1867m [8]).

3.1.2. Analysis of the tire

The force due to the elasticity of the tire [8];

$$F = -k_g x, \tag{3}$$

$$F = -k_g(l_{og} + R\mathrm{Sin}(\beta - \alpha_1) + r - D_x + U_{kin}). \tag{4}$$

k_g: The elasticity coefficient of the tire $(16000\mathrm{Nm}^{-1}$[8]).

U_{kin}: The input eccentricity.

x: The displacement of elasticity of the tire.

D_x: The distance between the pivot and the eccentric (0.2m [8]).

R: The distance between the MR damper and the center (0.2256m [8]).

The torque of tire elasticity [8];

$$T_{Tire_{Elasticity}} = -k_g R\mathrm{Cos}(\beta - \alpha_1)(l_{og} + R\mathrm{Sin}(\beta - \alpha_1) + r - D_x + U_{kin}). \tag{5}$$

The damping torque generated by the tire gum [8];

$$T_{Tire,\,Damping} = f_g \dot{x}. \tag{6}$$

$\dot{x}$: Derivation of the displacement of the tire elasticity.

f_g: Damping coefficient $(80\mathrm{Nsm}^{-1})$

$$T_{Tire,\,Damping} = f_g\left(\frac{d(D_x - U_{kin})}{dt} - \omega r\right); \tag{7}$$

$$T_{Tire,\,Damping} = f_g\left(\frac{d(D_x - U_{kin})}{dt} - \frac{d\alpha_1}{dt} R\mathrm{Cos}(\beta - \alpha_1)\right). \tag{8}$$

3.1.3. Equations for moments

The moment of the lower beam [8];

$$T_{Unsprung\ Mass} = J_1 \frac{d^2\alpha_1}{dt^2}. \tag{9}$$

The moment of the upper beam [8];

$$T_{Sprung\ Mass} = J_2 \frac{d^2\alpha_2}{dt^2}. \tag{10}$$

$J_1(0.1273\text{kgm}^{-2}$ [8]) and $J_2(1.1453\text{kgm}^{-2}$ [8]).

Viscous friction damping torque affecting on lower beam [8];

$$T_{Viscous} = k_1 \frac{d\alpha_1}{dt}. \tag{11}$$

k_1: The viscous friction coefficient lower beam $(1\text{Nsm}^{-1}$ [8]).

Viscous friction damping torque affecting on upper beam [8];

$$T_{Viscous} = k_2 \frac{d\alpha_2}{dt}. \tag{12}$$

k_2: The viscous friction coefficient upper beam $(0.3525\text{Nsm}^{-1}$ [8]).

Potential energy of the lower beam [8];

$$T_{Gravity\ Lower} = m_1 g_1 r_1 \text{Cos}(\beta - \alpha_1). \tag{13}$$

Potential energy of the upper beam [8];

$$T_{Gravity\ Upper} = m_2 g_2 r_2 \text{Cos}\,\alpha_2. \tag{14}$$

Kinetic energy of the spring [8];

$$T_{Spring} = r_2 K_s \left(l_{os} - \sqrt{(r_1 \text{Cos}\,\alpha_1 - r_2 \text{Cos}\,\alpha_2)^2 + (r_2 \text{Sin}\,\alpha_2 - r_1 \text{Sin}\,\alpha_1)^2} \right). \tag{15}$$

Elasticity spring torque of the tire [8];

$$T_{Tire\_Elasticity} = k_g R\text{Cos}(\beta - \alpha_1)(l_{og} + R\text{Sin}(\beta - \alpha_1) + r - D_x + U_{kin}). \tag{16}$$

The damping torque of the tire [8];

$$T_{Tire,\,Damping} = f_g\left(\frac{d(D_x - U_{kin})}{dt} - \frac{d\alpha_1}{dt} R\text{Cos}(\beta - \alpha_1)\right). \tag{17}$$

3.1.4. Analysis of upper beam

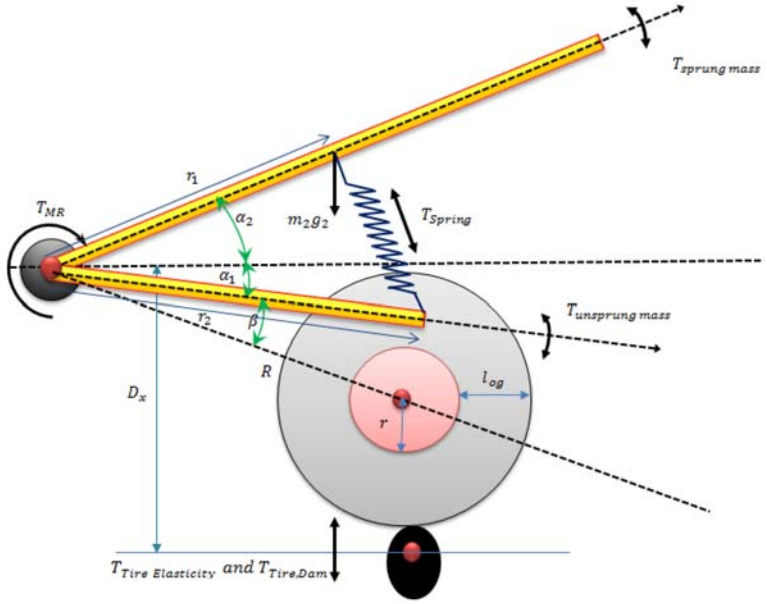

Figure 7. Torques acting on the SAS system effecting to the upper beam [8].

Newton's law;

$$\sum T_{sum} = J\dot{\omega}. \tag{18}$$

$$T_{sprung\ mass} = T_{Spring} - T_{Gravity\,Upper} - T_{Viscous} - T_{MR}. \tag{19}$$

$$J_2 \frac{d^2\alpha_2}{dt^2} + m_2 g_2 r_2 \mathrm{Cos}\,\alpha_2 - r_2 K_s \times \left(l_{os} - \sqrt{(r_1 \mathrm{Cos}\,\alpha_1 - r_2 \mathrm{Cos}\,\alpha_2)^2 + (r_2 \mathrm{Sin}\,\alpha_2 - r_1 \mathrm{Sin}\,\alpha_1)^2} \right) + k_2 \frac{d\alpha_2}{dt} = -C\left(\frac{d\alpha_1}{dt} - \frac{d\alpha_2}{dt} \right); \quad (20)$$

where C is damping coefficient of MR damper.

3.1.5. Analysis of lower beam

Newton's law;

$$\sum T_{sum} = J\dot{\omega}. \quad (21)$$

$$T_{unsprung\ mass} = -T_{Gravity\ lower} - T_{Spring} - T_{Viscous} + T_{Tire\_Elasticity} + T_{Tire,\ Damping} - T_{MR}. \quad (22)$$

$$J_1 \frac{d^2\alpha_1}{dt^2} + m_1 g_1 r_1 \mathrm{Cos}(\beta - \alpha_1) + r_1 K_s \left(l_{os} - \sqrt{(r_1 \mathrm{Cos}\,\alpha_1 - r_2 \mathrm{Cos}\,\alpha_2)^2 + (r_2 \mathrm{Sin}\,\alpha_2 - r_1 \mathrm{Sin}\,\alpha_1)^2} \right) + k_1 \frac{d\alpha_1}{dt} - k_g R \mathrm{Cos}(\beta - \alpha_1)(l_{og} + R\mathrm{Sin}(\beta - \alpha_1) + r - D_x + U_{kin}) - f_g \left(\frac{d(D_x - U_{kin})}{dt} - \frac{d\alpha_1}{dt} R \mathrm{Cos}(\beta - \alpha_1) \right) = -C\left(\frac{d\alpha_1}{dt} - \frac{d\alpha_2}{dt} \right) = -\left(\frac{d\alpha_1}{dt} - \frac{d\alpha_2}{dt} \right) M_{MR}. \quad (23)$$

3.2. Stability analysis of the SAS system

Two nonlinear, differential equations obtained for upper beam and lower beam, are used to find the equilibrium points of the SAS system. Stability is investigated though analytical methods illustrated in the Subsection 3.2.1.

3.2.1. Equilibrium points

Linearizing nonlinear system,

$$\alpha_1 = y_1,$$

$$\dot{\alpha}_1 = y_2 = \dot{y}_1,$$

$$\alpha_2 = y_3,$$

$$\dot{\alpha}_2 = y_4 = \dot{y}_3.$$

Using Equation (20);

$$J_2\dot{y}_4 + m_2g_2r_2\text{Cos}\, y_3 - r_2K_s\left(l_{os} - \sqrt{(r_1\text{Cos}\, y_1 - r_2\text{Cos}\, y_3)^2 + (r_2\text{Sin}\, y_3 - r_1\text{Sin}\, y_1)^2}\right)$$

$$+ k_2y_4 = -(y_2 - y_4)M_{MR}(i),$$

$$\dot{y}_4 = \frac{1}{J_2}\Big[-(y_2 - y_4)M_{MR}(i) - m_2g_2r_2\text{Cos}\, y_3 + r_2K_s$$

$$\times\left(l_{os} - \sqrt{(r_1\text{Cos}\, y_1 - r_2\text{Cos}\, y_3)^2 + (r_2\text{Sin}\, y_3 - r_1\text{Sin}\, y_1)^2}\right) - k_2y_4\Big] = A.$$

Using Equation (23);

$$J_1\dot{y}_2 + m_1g_1r_1\text{Cos}(\beta - y_1)$$

$$+ r_1K_s\left(l_{os} - \sqrt{(r_1\text{Cos}\, y_1 - r_2\text{Cos}\, y_3)^2 + (r_2\text{Sin}\, y_3 - r_1\text{Sin}\, y_1)^2}\right)$$

$$+ k_1y_2 - k_gR\text{Cos}(\beta - y_1)(l_{og} + R\text{Sin}(\beta - y_1) + r - D_x + U_{kin})$$

$$- f_g\left(\frac{d(D_x - U_{kin})}{dt} - y_2R\text{Cos}(\beta - y_1)\right) = -(y_2 - y_4)M_{MR}(i),$$

$$\dot{y}_2 = \frac{1}{J_1}\Big[-(y_2 - y_4)M_{MR}(i) - m_1g_1r_1\text{Cos}(\beta - y_1) - r_1K_s$$

$$\times\left(l_{os} - \sqrt{(r_1\text{Cos}\, y_1 - r_2\text{Cos}\, y_3)^2 + (r_2\text{Sin}\, y_3 - r_1\text{Sin}\, y_1)^2}\right)$$

$$- k_1y_2 + k_gR\text{Cos}(\beta - y_1)(l_{og} + R\text{Sin}(\beta - y_1) + r - D_x + U_{kin})$$

$$+ f_g\left(\frac{d(D_x - U_{kin})}{dt} - y_2 R\mathrm{Cos}(\beta - y_1)\right)\Big]$$

$$= B.$$

In matrix form $\dot{Y} = f(y, t)$

$$\begin{bmatrix}\dot{y}_1\\ \dot{y}_2\\ \dot{y}_3\\ \dot{y}_4\end{bmatrix} = \begin{bmatrix}y_2\\ B\\ y_4\\ A\end{bmatrix}.$$

To find the equilibrium point, $\dot{Y} = 0$

$$\dot{\alpha}_1 = y_2 = \dot{y}_1 = 0,$$

$$\dot{\alpha}_2 = y_4 = \dot{y}_3 = 0,$$

$$A = 0 \text{ and } B = 0.$$

$$\frac{1}{J_2}\Big[-(y_2 - y_4)M_{MR}(i) - m_2 g_2 r_2 \mathrm{Cos}\, y_3 + r_2 K_s$$

$$\times\left(l_{os} - \sqrt{(r_1\mathrm{Cos}\, y_1 - r_2\mathrm{Cos}\, y_3)^2 + (r_2\mathrm{Sin}\, y_3 - r_1\mathrm{Sin}\, y_1)^2}\right) - k_2 y_4\Big] = 0. \tag{24}$$

$$\frac{1}{J_1}\Big[-(y_2 - y_4)M_{MR}(i) - m_1 g_1 r_1 \mathrm{Cos}(\beta - y_1) - r_1 K_s$$

$$\times\left(l_{os} - \sqrt{(r_1\mathrm{Cos}\, y_1 - r_2\mathrm{Cos}\, y_3)^2 + (r_2\mathrm{Sin}\, y_3 - r_1\mathrm{Sin}\, y_1)^2}\right)$$

$$- k_1 y_2 + k_g R\mathrm{Cos}(\beta - y_1)(l_{og} + R\mathrm{Sin}(\beta - y_1) + r - D_x + U_{kin})$$

$$+ f_g\left(\frac{d(D_x - U_{kin})}{dt} - y_2 R\mathrm{Cos}(\beta - y_1)\right)\Big] = 0. \tag{25}$$

For the equilibrium;

$$(24) * r_2 + (25) * r_1 = 0. \tag{26}$$

$$\left[- m_1 g_1 r_1 \mathrm{Cos}(\beta - y_1) + k_g R \mathrm{Cos}(\beta - y_1)(l_{og} + R\mathrm{Sin}(\beta - y_1) + r - D_x + U_{kin}) \right.$$

$$\left. + f_g\left(\frac{d(D_x - U_{kin})}{dt}\right) \right] * r_2 - [- m_2 g_2 r_2 \mathrm{Cos}\, y_3] * r_1 = 0. \tag{27}$$

It is not possible to find exact values for the α_1 and α_2 due to analytical limitations in analytical methods.

3.2.2. Stability investigation

At the position of current input to the MR damper is zero, the upper beam is given an initial excitation (α_2) of 20 degrees and the lower beam is kept at the default position (α_1), – 3.653 degrees [8]. Measured α_1 and α_2 values are plotted as in the Figures 8 and 9, respectively.

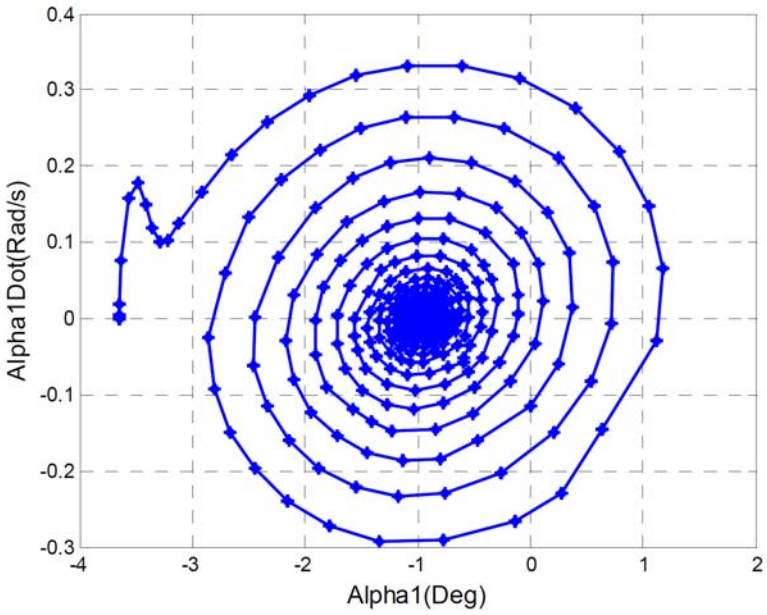

Figure 8. Velocity vs. displacement at I = 0A for lower beam.

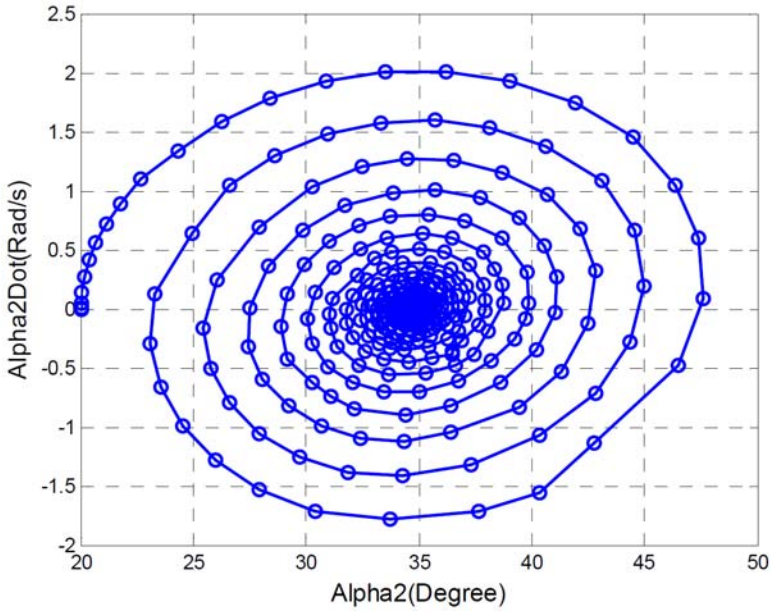

Figure 9. Velocity vs. displacement at $I = 0$A for upper beam.

From the plots, it can be seen that trajectories are spiral into the equilibrium from an outside position. Thus, it can be concluded that the equilibrium point of $\alpha_1 = -1$ deg and the equilibrium point of $\alpha_2 = 34$ deg are both stable equilibrium points.

4. The Bouc-Wen Model for MR Dampers

A parametric model; Bouc-Wen model [3] is analyzed to describe the hysteresis; torque vs velocity and torque vs displacement behaviour of the MR damper.

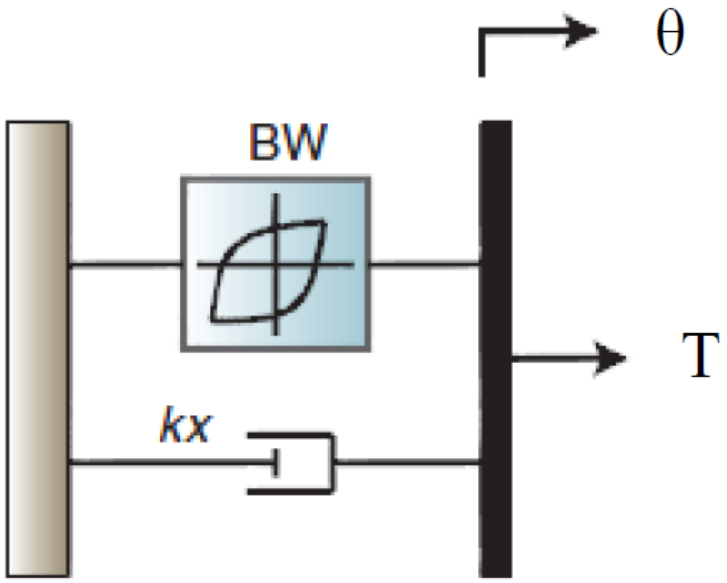

Figure 10. The Bouc-Wen model [3].

Torque (T) generated by the MR damper, in response to a displacement (θ) is given by [7];

$$T = \alpha(i)z + C(i)\dot{\theta},$$

$$\dot{z} = -\gamma|\dot{\theta}|z|z|^{n-1} - \beta\dot{\theta}|z|^{n} + \delta\dot{\theta},$$

$$C(i) = C_1 + C_2 i,$$

$$\alpha(i) = \alpha_1 + \alpha_2 i,$$

α, C: Damping coefficients depends on current i.

γ, β, δ, n: Parameters which control the shape of hysteresis.

z: Hysteretic displacement.

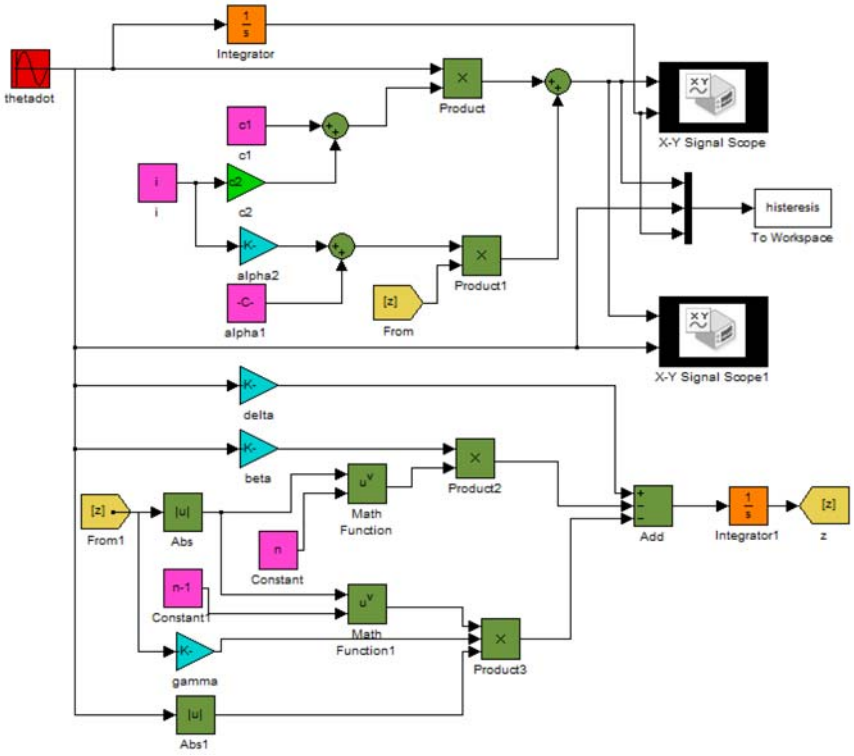

Figure 11. Matlab simulink model of Bouc-Wen.

4.1. Hysteresis behaviour

Bouc-Wen model parameters, which have been used to determine, "MR damper hysteresis characterization for the semi active suspension system" [8] are applied and results are obtained for zero current.

$\gamma = 1$, $\beta = 737$, $\delta = 843$, $n = 1.9$, $C_1 = 0.0015$, $C_2 = 17$, $\alpha_1 = 1$, $\alpha_2 = 17$.

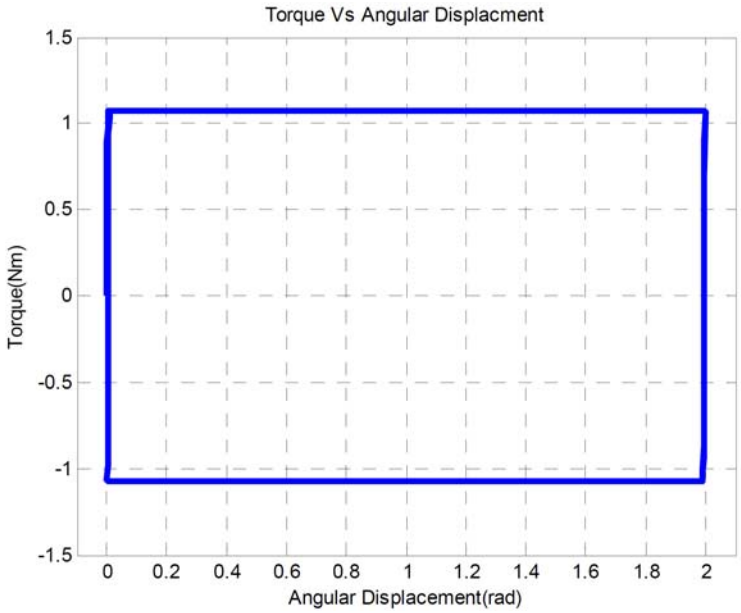

Figure 12. Torque vs. displacement hysteresis.

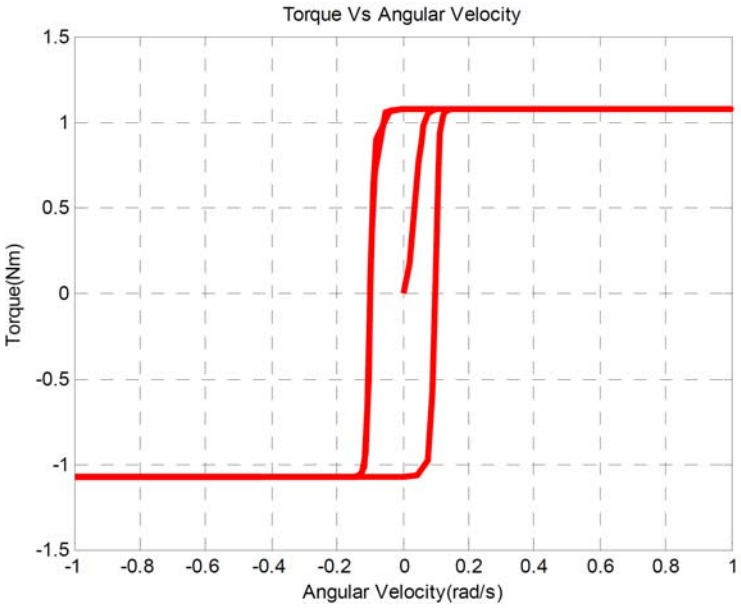

Figure 13. Torque vs. velocity hysteresis.

4.2. Effect of the current on the hysteresis behaviour

As per the behaviour it becomes quite evident, when the current increases, torque also increases, i.e., the effect of current obviously changes the damping effect. However, it can be clearly seen that there is a negligible effect of current to change the width of the hysteresis curve as the width remains almost at the same dimension.

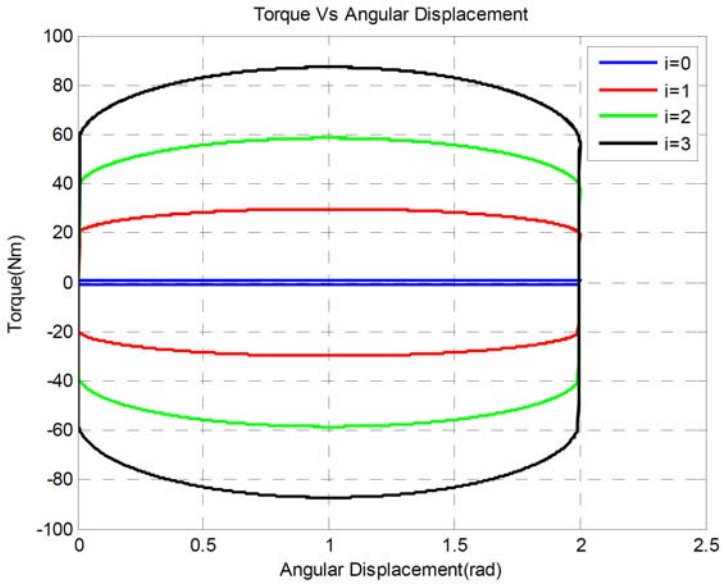

Figure 14. Torque vs. displacement hysteresis for different currents.

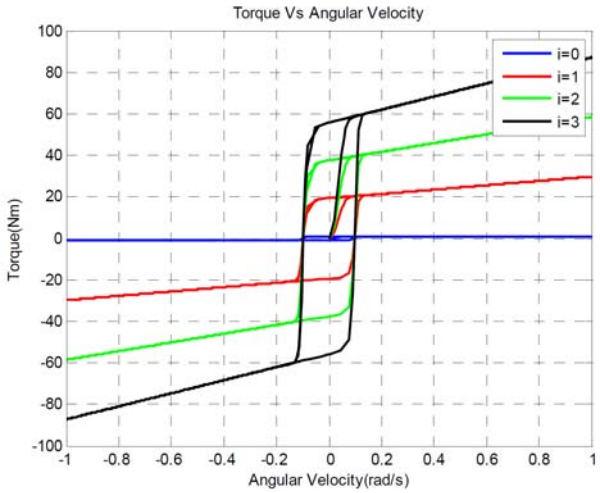

Figure 15. Torque vs. velocity hysteresis for different currents.

4.3. Effect of MR damper parameters on the hysteresis behaviour

The hysteresis curves for different values of γ, β, δ, and n are obtained for control currents 0A and 2A from simulink model as per the below.

Effect of γ

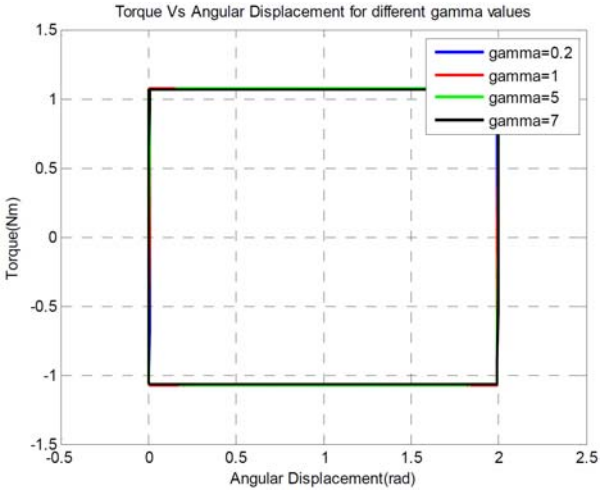

Figure 16. Displacement hysteresis for different γ values at current 0A.

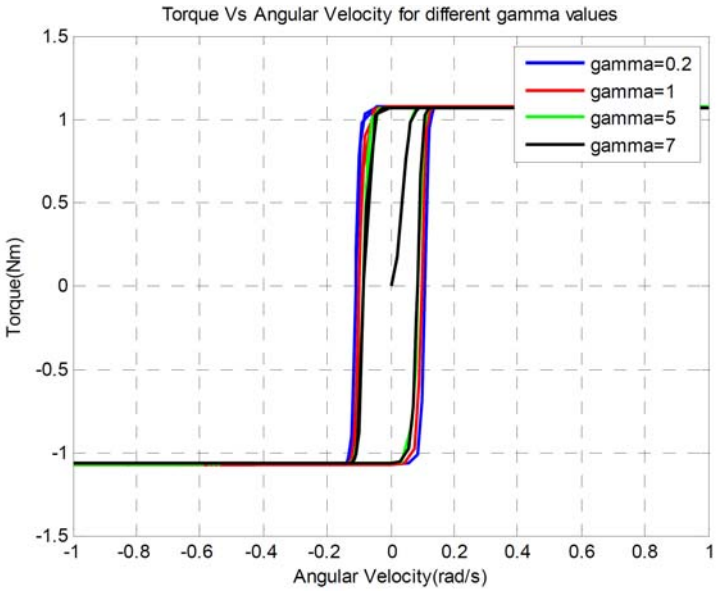

Figure 17. Velocity hysteresis for different γ values at current 0A.

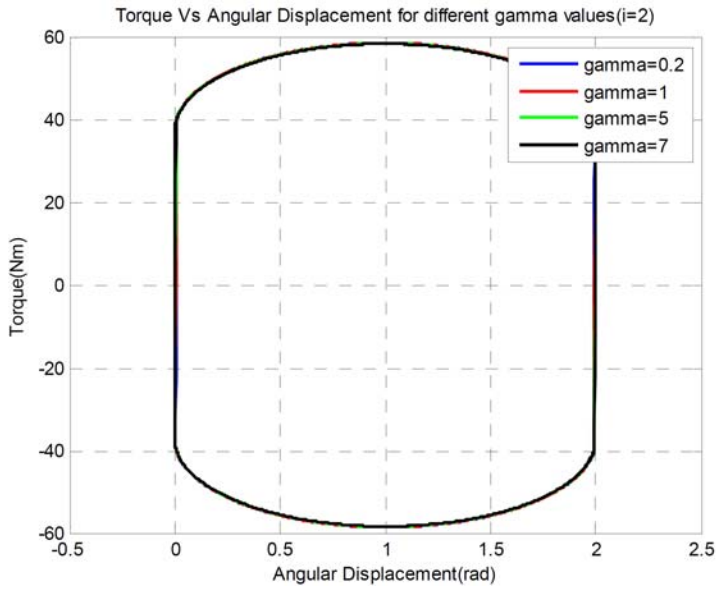

Figure 18. Displacement hysteresis for different γ values at current 2A.

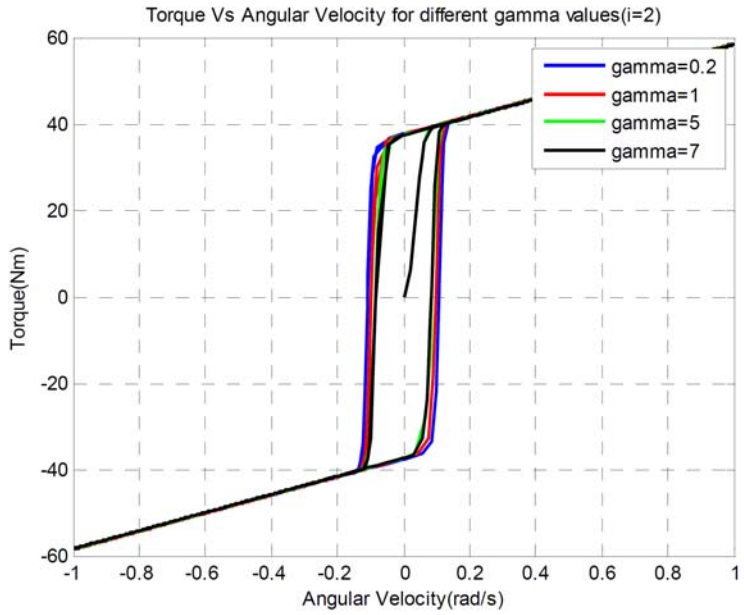

Figure 19. Velocity hysteresis for different γ values at current 2A.

As per the results, it can be seen, when the γ changes it has almost negligible effect on the torque with respect to displacement and angular velocity for two control currents, 0A and 2A. However, it is revealed that the width of the hysteresis curve decreases when γ increases with respect to velocity hysteresis.

Effect of β

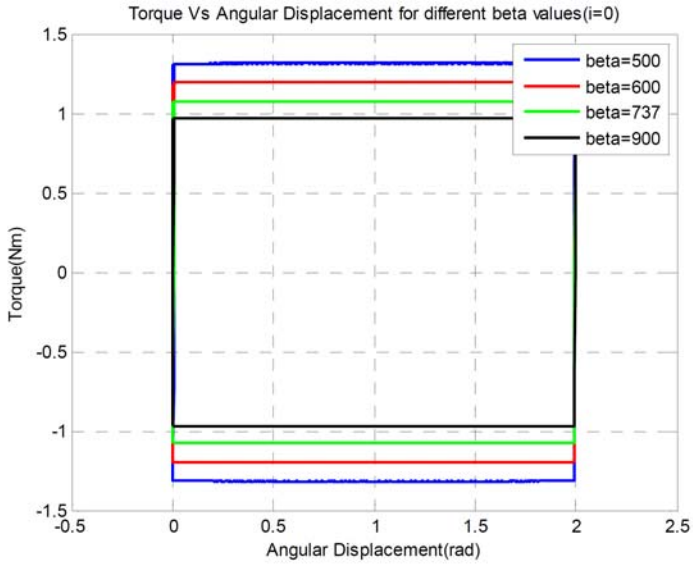

Figure 20. Displacement hysteresis for different β values at current 0A.

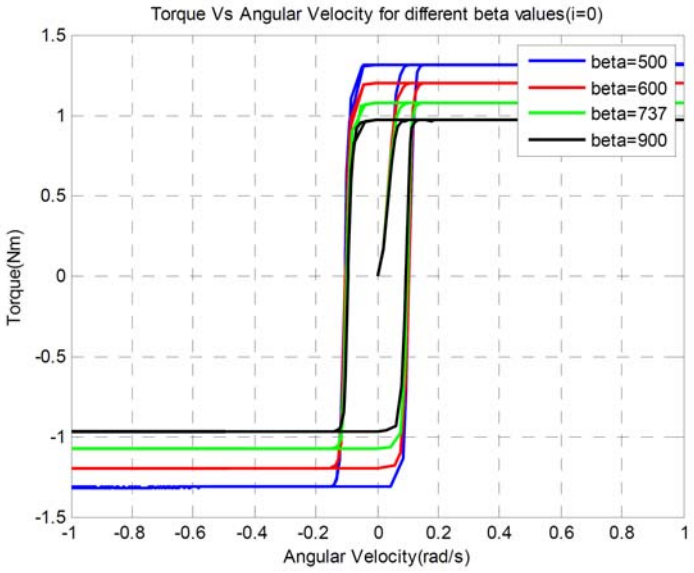

Figure 21. Velocity hysteresis for different β values at current 0A.

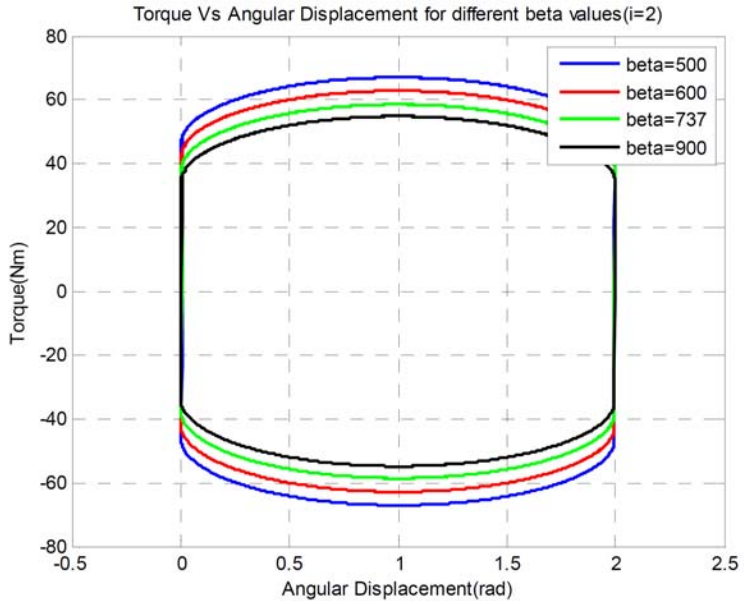

Figure 22. Displacement hysteresis for different β values at current 2A.

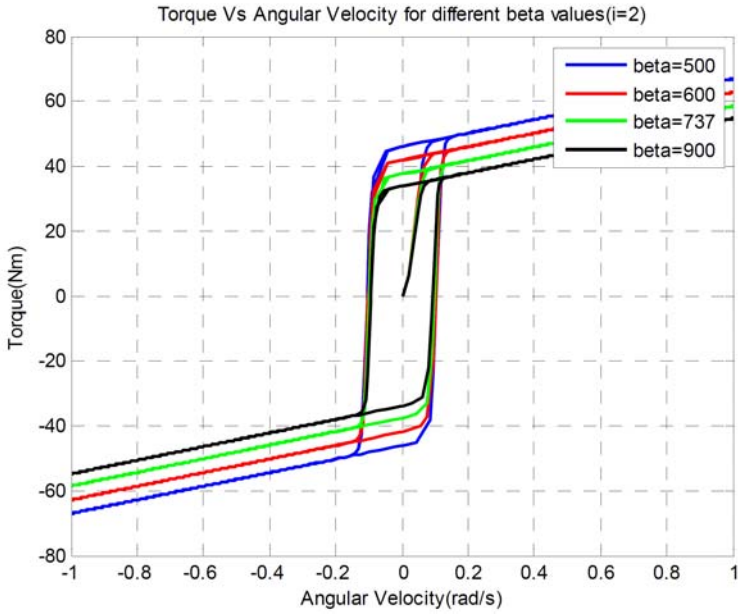

Figure 23. Velocity hysteresis for different β values at current 2A.

It is revealed that, the height of both, displacement hysteresis and velocity hysteresis decreases when β increases. Hence, MR damper torque can be increased by decreasing β.

Effect of δ

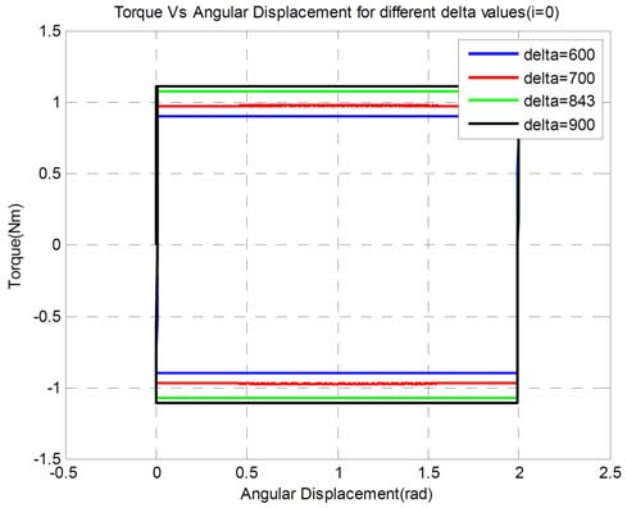

Figure 24. Displacement hysteresis for different δ values at current 0A.

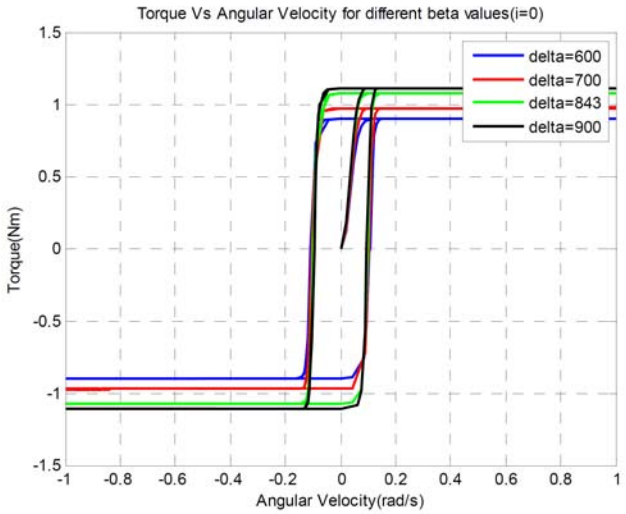

Figure 25. Velocity hysteresis for different δ values at current 0A.

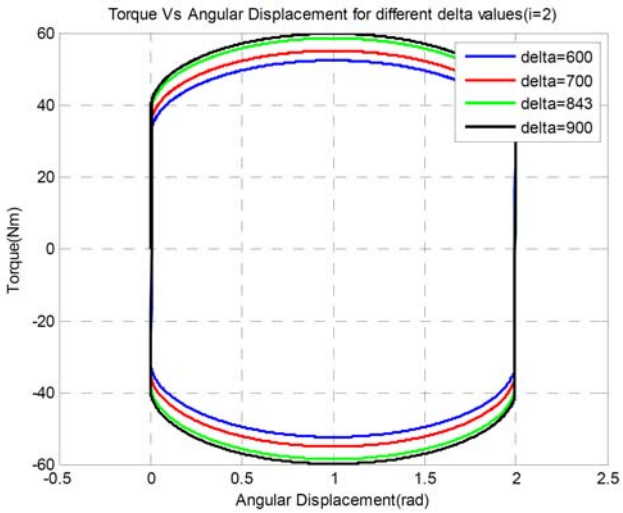

Figure 26. Displacement hysteresis for different δ values at current 2A.

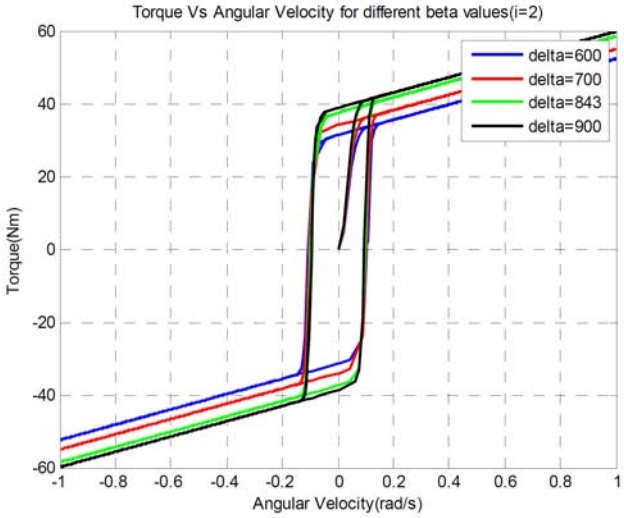

Figure 27. Velocity hysteresis for different δ values at current 2A.

As per the results, it is obvious that, increase in n decreases the height of the displacement and velocity hysteresis. It can be concluded that the torque of the MR damper could be reduced by increasing the parameter n.

4.4. Vibration response of the SAS system with Bouc-Wen

The Bouc-Wen model is connected to the SAS simulation model as in the Figure 28 and vibration response is determined by fixing the lower beam (α_1) at an angle of 0 degree and the upper beam at an angle of 17.14 degrees (α_2). The vibration response is obtained for different MR damper parameters setting control current to 0.25A.

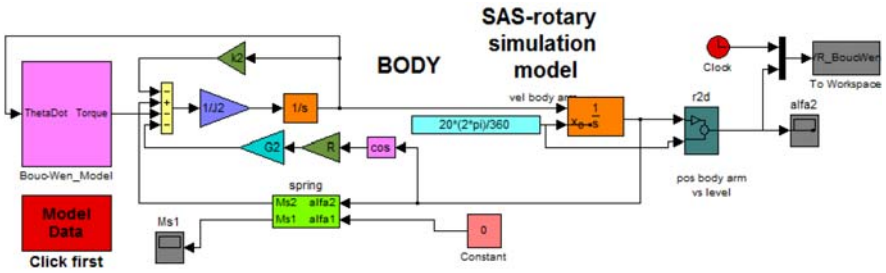

Figure 28. Simulink model for SAS system with Bouc-Wen, setting $\alpha_1 = 0$.

4.5. Effect of MR damper parameters on the vibration response of the system

Effect of γ

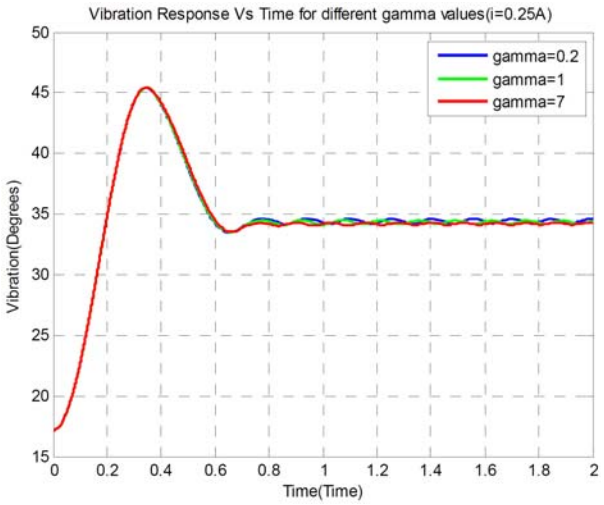

Figure 29. Position of the upper beam for different γ values.

Effect of β

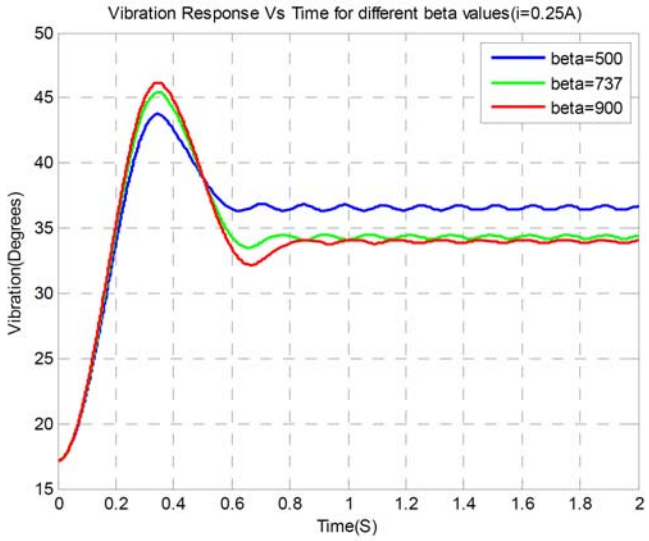

Figure 30. Position of the upper beam for different β values.

Effect of δ

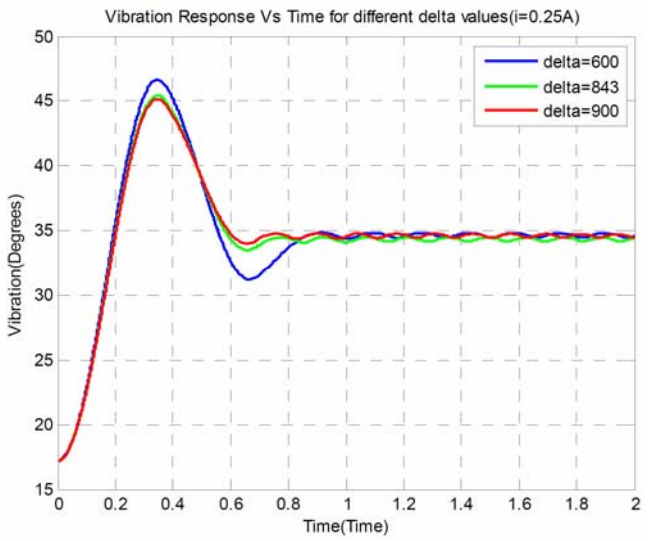

Figure 31. Position of the upper beam for different δ values.

Effect of *n*

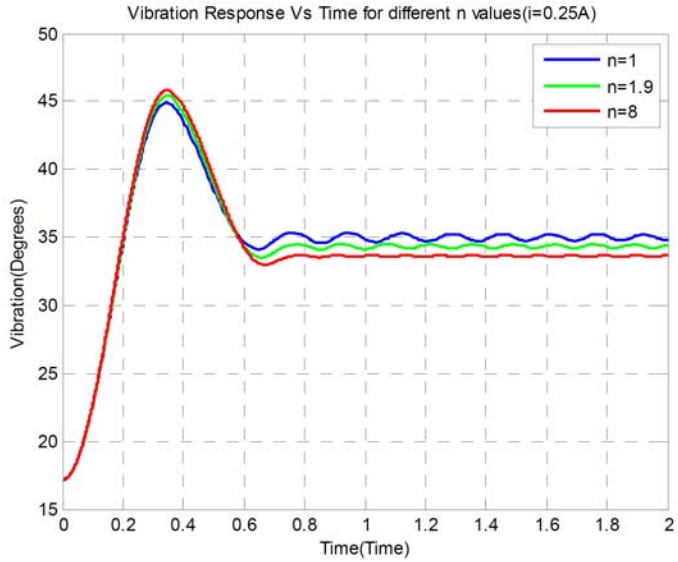

Figure 32. Position of the upper beam for different n values.

Effect of C_2

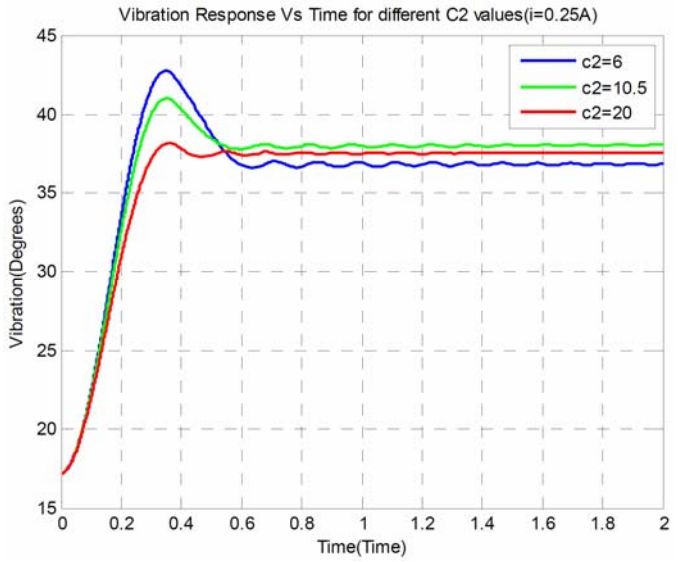

Figure 33. Position of the upper beam for different c_2 values.

Effect of α_2

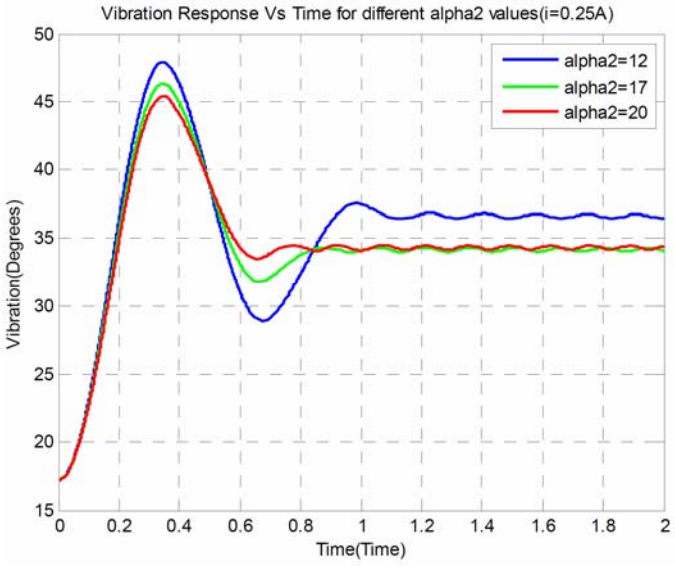

Figure 34. Position of the upper beam for different α_2 values.

Observations depict changes in the parameters of the Bouc-Wen model affect to the steady state response time and the steady state value of the body position. It is obvious that the vibration response is not dramatically affected by small changes in γ, δ, and n. However, changes in β, c_2 and α_2 have a quite significant impact to the steady state response of the system. Also, steady state response time is largely reduced when c_2 is increased.

5. Comparison of Vibration Responses Between the Experimental Measurements and the Theoretical; Bouc-Wen Model

The SAS platform which is depicted in Figure 5 is used for these measurements. Lower beam of the system is clamped, setting α_1 to zero degrees and the upper beam is compressed to a fixed position and released in each stage of measurement. The vibration responses are obtained for different MR damper control currents, I = 0A to I = 1.5A.

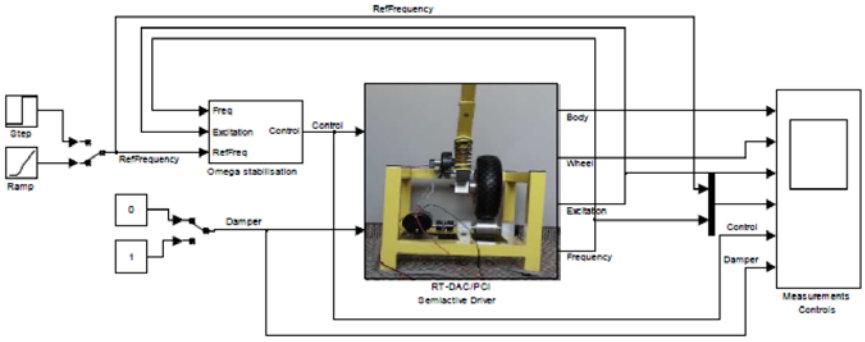

Figure 35. Simulink diagram of the SAS controller.

Vibration response obtained from the experiment is compared with the vibration response with the theoretical; Bouc-Wen model connected to SAS system. The results are plotted for two control current inputs, I = 0.25A and I = 1A as shown in the Figures 36 and 37, respectively.

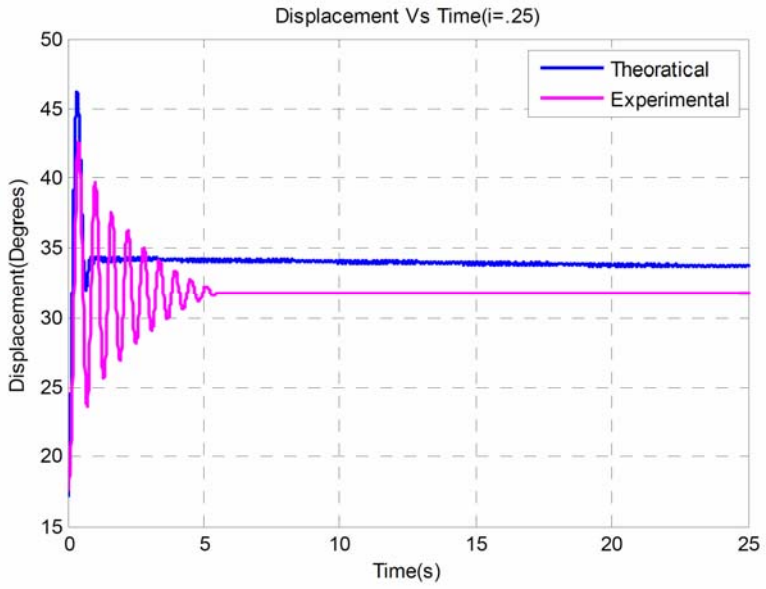

Figure 36. Vibration response for the theoretical; Bouc-Wen and the experimental measurement at 0.25A.

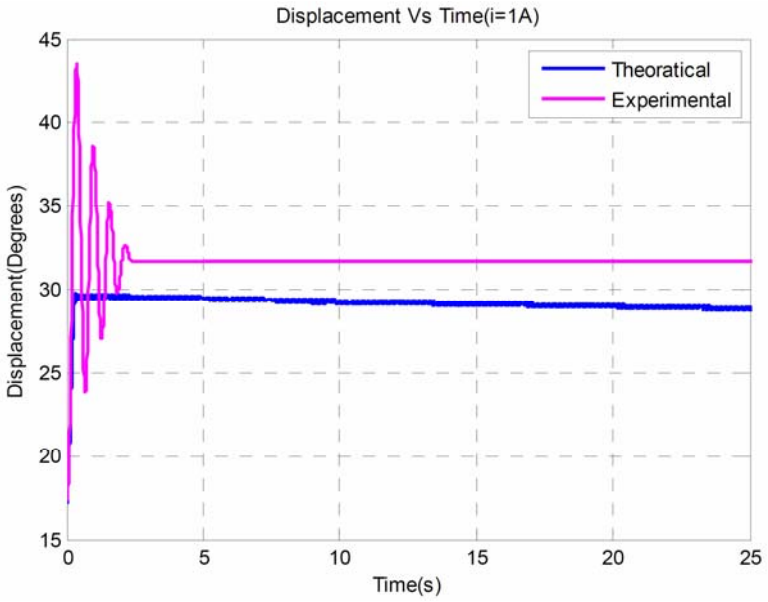

Figure 37. Vibration response for the theoretical; Bouc-Wen and the experimental measurement at 1.0A.

It can be seen that both experimental and Bouc-Wen attain approximately close steady state value at the equilibrium.

6. Conclusion

The SAS is a portable device operating in the MATLAB Simulink environment. By using SAS test rig, it is easy to analyze the control results corresponding to effects of parameters in proposed models and steady state responses of the MR damper. It is revealed that the experimental results slightly diverge from the theoretical results for the applied parameters of Bouc-Wen model. Further it is found; when model parameters are diligently tuned it is possible to overlap the results of experimental displacement with theoretical displacement around the stability point of the upper beam (α_2) 34 degrees. Bouc-Wen has exponential terms and more parameters allowing tuning more sophisticatedly, which drives the model into more advanced nonlinear

one. Therefore, it can be concluded that, Bouc-Wen model stands at a premier level as far as the more realistic accurate results are concerned. As a future research, it is recommended, modelling of the SAS with MR rotary damper developing more effective control algorithms, which would be tested in a wide frequency domain, operating in real time. In conclusion, the test results witness that the magnitude of vibrations, especially in the neighbourhood of the resonance frequency is significantly reduced with MR dampers. All in all, it is obvious that the semi-active dampers provide remarkable improvements over passive suspensions.

References

[1] Y. Iskandarani, G. A. Moslatt, E. Myklebust, J. P. Kolberg, L. L. Solberg and H. R. Karimi, Hysteresis identification methodology for the SAS rotational MR damper, WSEAS Transactions on Applied and Theoretical Mechanics 6(4) (2011), 137-146.

[2] Arturo Rodriguez Tsouroukdissian, Faycal Ikhouane, Jose Rodellar and Ningsu Luo, Modeling and identification of a small-scale magneto-rheological damper, Journal of Intelligent Material Systems and Structures 20(7) SAGE, (2009), 825-835.

[3] B. F. Spencer Jr., S. J. Dyke, M. K. Sain and J. D. Carlson, Phenomenological model for magneto-rheological dampers, Journal of Engineering Mechanics 123(3) (1997), 230-238.

[4] Thomas Avraam, MR-Fluid Brake Design and its Application to a Portable Muscular Rehabilitation Device, Ph.D. Dissertation, Active Structures Laboratory, Department of Mechanical Engineering and Robotics, Universitélibre de Bruxelles, 2009.

[5] F. D. Goncalves, M. Ahmadian and J. D. Carlson, Characterizing the behavior of magneto-rheological fluids at high velocities and high shear rates, International Journal of Modern Physics B 19(7-9) (2005), 1395-1401.

[6] James Poynor, Innovative Designs for Magneto-Rheological Dampers, Master's Thesis, Advanced Vehicle Dynamics Laboratory, Virginia Polytechnic Institute and State University, 2001.

[7] I. S. Ahin, T. Engin and S. C. Esmeci, Comparison of some existing parametric models for magneto-rheological fluid dampers, Smart Materials and Structures 19(3) (2010).

[8] Dariush Ghorbany, MR Damper Hysteresis Characterization for the Semi-Active Suspension System, Master's Thesis in Mechatronics, Department of Engineering, Faculty of Engineering Science, University of Agder, 2011.

[9] Hamid Reza Karimi, A Semiactive Vibration Control Design for Suspension Systems with MR Dampers, Vibration Analysis and Control-New Trends and Developments, Dr. Francisco Beltran-Carbajal (Ed.), ISBN: 978-953-307-433-7 (2011); InTech, Available from:

http://www.intechopen.com/books/vibration-analysis-and-controlnew-trends-and-developments/a-semiactive-vibration-control-design-for-suspension-systems-withmrdampers.

[10] John W. Gravatt, Magneto-Rheological Dampers for Super Sport Motorcycle Applications, Master's Thesis, Faculty of the Virginia Polytechnic Institute and State University, 2003.

[11] Min-Sang Seong, Seung-Bok Choi and Kum-Gil Sung, Control Strategies for Vehicle Suspension System Featuring Magneto-Rheological (MR) Damper, Vibration Analysis and Control-New Trends and Developments, Dr. Francisco Beltran-Carbajal (Ed.), ISBN: 978-953-307-433-7 (2011); InTech, Available from:

http://www.intechopen.com/books/vibration-analysis-and-control-new-trends-and-developments/controlstrategies-for-vehicle-suspension-system-featuring-magnetorheological-mr-damper.

■